

Investigation of Chemical-Foam Design as a Novel Approach toward Immiscible Foam Flooding for Enhanced Oil Recovery

Hosseini-Nasab, S. M.; Zitha, P. L.J.

DOI

[10.1021/acs.energyfuels.7b01535](https://doi.org/10.1021/acs.energyfuels.7b01535)

Publication date

2017

Document Version

Final published version

Published in

Energy & Fuels

Citation (APA)

Hosseini-Nasab, S. M., & Zitha, P. L. J. (2017). Investigation of Chemical-Foam Design as a Novel Approach toward Immiscible Foam Flooding for Enhanced Oil Recovery. *Energy & Fuels*, 31(10), 10525-10534. <https://doi.org/10.1021/acs.energyfuels.7b01535>

Important note

To cite this publication, please use the final published version (if applicable). Please check the document version above.

Copyright

Other than for strictly personal use, it is not permitted to download, forward or distribute the text or part of it, without the consent of the author(s) and/or copyright holder(s), unless the work is under an open content license such as Creative Commons.

Takedown policy

Please contact us and provide details if you believe this document breaches copyrights. We will remove access to the work immediately and investigate your claim.



Investigation of Chemical-Foam Design as a Novel Approach toward Immiscible Foam Flooding for Enhanced Oil Recovery

S. M. Hosseini-Nasab*[✉] and P. L. J. Zitha

Delft University of Technology, Department of Geoscience & Engineering, Petroleum Engineering Group, Delft, Netherlands

ABSTRACT: Strong foam can be generated in porous media containing oil, resulting in incremental oil recovery; however, oil recovery factor is restricted. A large fraction of oil recovered by foam flooding forms an oil-in-water emulsion, so that costly methods may need to be used to separate the oil. Moreover, strong foam could create a large pressure gradient, which may cause fractures in the reservoir. This study presents a novel chemical-foam flooding process for enhanced oil recovery (EOR) from water-flooded reservoirs. The presented method involved the use of chemically designed foam to mobilize the remaining oil after water flooding and then to displace the mobilized oil to the production well. A blend of two anionic surfactant formulations was formulated for this method: (a) IOS, for achieving ultralow interfacial tension (IFT), and (b) AOS, for generating a strong foam. Experiments were performed using Bentheimer sandstone cores, where X-ray CT images were taken during foam generation to find the stability of the advancing front of foam propagation and to map the gas saturation for both the transient and the steady-state flow regimes. Then the proposed chemical-foam strategy for incremental oil recovery was tested through the coinjection of immiscible nitrogen gas and surfactant solutions with three different formulation properties in terms of IFT reduction and foaming strength capability. The discovered optimal formulation contains a foaming agent surfactant, a low IFT surfactant, and a cosolvent, which has a high foam stability and a considerably low IFT (1.6×10^{-2} mN/m). Coinjection resulted in higher oil recovery and much less MRF than the same process with only using a foaming agent. The oil displacement experiment revealed that coinjection of gas with a blend of surfactants, containing a cosolvent, can recover a significant amount of oil (33% OIIP) over water flooding with a larger amount of clean oil and less emulsion.

1. INTRODUCTION

Gas injection for enhanced oil recovery (EOR) suffers from poor sweep efficiency due to three main reasons: (1) gas segregation and gravity override due to a lower density of gas than oil and water phases, (2) viscous fingering due to a high mobility ratio between gas and oil or water, and (3) gas channelling through high-permeability zones in heterogeneous and layered reservoirs.^{1,2} Foam diminishes gas mobility leading to a substantial rise of the pressure gradient and consequently improves volumetric sweep efficiency by such reduction of gas mobility. Thus, foam provides a favorable mobility ratio between drive (gas) and displaced (oil and water) fluids and contacts a larger fraction of the reservoir to mitigate the effect of heterogeneity, gas segregation, and viscous instability.^{3,4} Foam for EOR is implemented either by coinjection of gas and surfactant or by surfactant alternating gas (SAG) injection. Gas and surfactant coinjection leads to far larger mobility reduction than SAG injection.^{5,6}

Foam has also been identified as a suitable alternative to polymer in an alkaline–surfactant–polymer (ASP) flooding EOR process for reservoir formation with a low permeability and a high heterogeneity. Alkali–surfactant–foam (ASF) flooding is a new EOR method, which applies foam as a mobility control agent instead of polymer.^{7,8} Moreover, the presence of alkaline–surfactant (AS) slug creates a base (high pH) environment and in situ soap generation, which enables a significant reduction of IFT and surfactant adsorption.^{9–11} IFT reduction during foam floods leads to an increase of the capillary number, thus improving microscopic displacement of oil.^{7,12} Similar processes to ASF flooding have been reported by others under different terminology, for instance, low tension

gas (LTG) and alkali–surfactant gas (ASG) flooding.^{13–15} For ASF flooding in water-flooded reservoirs, foam can divert AS slug to low-permeability layers, thus mobilizing trapped residual oil by lowering IFT and by reducing capillary forces.^{16,17}

Advantages of foam over polymers include the fact that foam can divert flow from high-permeable regions to low-permeable zones, thus leading to improved sweep efficiency and higher oil recovery factors.^{18,19} This is due to the fact foam is stronger, which is more fine texture and stable, in high-permeability zones than in low-permeability oil-bearing zones.^{20–23} The efficiency of immiscible foam flooding as an EOR method is limited. Although strong foam can be generated in the presence of oil, incremental oil recovery by the foam flooding on a tertiary recovery mode does not exceed 30% of OIIP in a reasonable number of pore volumes of foam injection. Moreover, a large fraction of oil recovered by foam flooding forms a stable oil-in-water emulsion, so that separating the oil out may require costly methods.

This study investigates the impact of the IFT reduction, foam mobility reduction, and synergetic effect of these two factors on the performance of foam flooding. Our aim is to shed more light into foam behavior, especially in terms of microscopic displacement of trapped oil and volumetric sweep efficiency, which is of great importance. To achieve this, the formulation of a foaming agent capable of producing ultralow IFT between oil and water and at the same time generate a stable foam has

Received: May 30, 2017

Revised: August 25, 2017

Published: August 28, 2017

been examined in detail. The structure of this paper is as follows. First, we present the experimental materials and methods including the core-flooding procedure, CT scan setting, and processing. The paper proceeds with the results and discussions of foam flooding for chemical formulations in sandstone porous media without oleic phase. Next, the results of core-flooding experiments for EOR are presented and discussed. Finally, the main conclusions are drawn.

2. EXPERIMENTAL DESCRIPTION

2.1. Materials. Brine was prepared by adding sodium chloride (NaCl, Merck) and sodium carbonate (Na_2CO_3) both at a fixed concentration of 1.0 wt % to demineralized water. The density and viscosity of brine thus prepared at 25 °C were $1.07 \pm 0.01 \text{ g/cm}^3$ and $1.10 \pm 0.01 \text{ cP}$, respectively. The used surfactants were alpha olefin sulfonate (AOS) and internal olefin sulfonate (IOS, Shell Chemical) with a long carbon chain. AOS and IOS surfactants were supplied as a liquid with 40 and 19 wt % active content, respectively, and they were used as received without further treatment. The cosolvent was a *sec*-butyl alcohol (SBA, Merck, 99% pure). The critical micelle concentrations (cmc's) of AOS and IOS solutions in the presence of 2.5 wt % NaCl were 3.5×10^{-3} and 5×10^{-3} wt %, respectively. Normal hexadecane (n-C16, Sigma-Aldrich) with a purity larger than 99 wt % was used as model oil. The viscosity and density of *n*-hexadecane at 25 °C were found to be $3.2 \pm 0.01 \text{ cP}$ and $0.78 \pm 0.01 \text{ g/cm}^3$, respectively. Nitrogen gas used had a purity of 99.98% for foam generation. The surfactant viscosity was 1.08 mPa·s. The properties of Bentheimer core are summarized in Table 1. The setup used to conduct the core-flooding experiments is shown schematically in Figure 1.

Table 1. Physical Properties of the Core Samples Used for Core-Flood Test

core sample	Bentheimer sandstone
porosity (%)	23.0 ± 0.1
diameter (cm)	3.8 ± 0.1
length (cm)	17.0 ± 0.1
pore volume (cm^3)	46.5 ± 0.5
brine permeability (Darcy)	2.5 ± 0.1
quartz content of rock (wt %)	92.0 ± 1.0

2.2. CT Scan Setting and Processing. X-ray CT images presented in this study were obtained using the medical CT scanner,

SOMATOM definition. CT scanning is based on the attenuation of X-ray beams through the object being scanned. The attenuation coefficient is different for the local physical properties and concentrations of the materials scanned. CT scanners provide image matrices where the attenuation coefficients are expressed in Hounsfield units (CT numbers) defined as

$$CT = 1000 \left(\frac{\mu}{\mu_w} - 1 \right) \quad (1)$$

where CT is the CT-number value in Hounsfield unit, μ_w is the X-ray attenuation coefficient of water (units of m^{-1}), and μ is the X-ray linear attenuation coefficient of the sample (units of m^{-1}). The settings used for CT images in the experiments are listed in Table 2. The CT

Table 2. Setting Parameters for the CT Scan Measurements

parameter (units)	value/condition
tube current (mA)	250
tube voltage (kV)	140
pixel (voxel) size (mm × mm)	0.195×0.195
slice thickness (mm)	3.0
filter	B40-medium
scan mode	sequential

scanner took 4 images at each scan vertically from top to bottom of the core with a slice thickness of 3 mm. The sequential scan mode was used for imaging acquisition, as it provides a low noise-to-signal ratio. The spatial resolution of CT was based on the voxel volume that was $0.195 \times 0.195 \times 0.6 \text{ mm}$. The highest resolution of the image display was 512×512 pixels.

To calculate rock porosity and fluid saturations inside the rock, we used the method presented in the work of Rangel-German et al. (1999). The porosity ϕ of the core samples can be calculated by using CT images of dry core and fully brine-saturated core and the CT number (Hounsfield unit) values of brine and air

$$\phi = \frac{CT_{\text{wet}} - CT_{\text{dry}}}{CT_w - CT_g} \quad (2)$$

where CT_{wet} , CT_{dry} , CT_w , and CT_g are, respectively, the measured attenuation coefficients for fully water-saturated core, dry core, water, and air. For the drainage process (oil injection) and the imbibition (water flooding) experiments, due to combined effects of rock, the water phase, and the oleic phase, one can write for each voxel of rock sample the following equation to calculate the oil in situ saturation

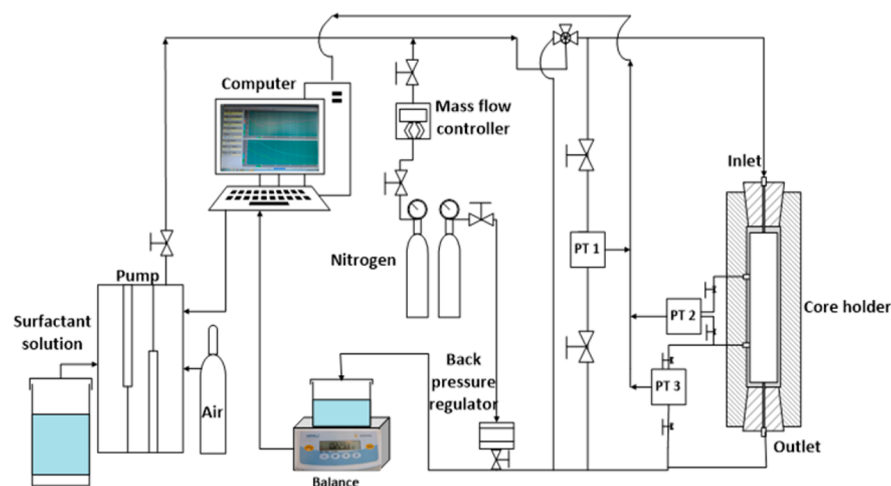


Figure 1. Schematic overview of the core-flooding setup for foam flow and oil displacement experiment used in CT scan visualization. Core holder was placed vertically on the table of CT scanner.

$$S_o = \frac{1}{\varphi} \frac{CT - CT_{wet}}{CT_o - CT_w} \quad (3)$$

During foam flooding, the attenuation coefficient of the core plug is a combination of the gas-phase and the liquid-phase attenuation coefficients. To describe the in situ distribution of gas–liquid systems, the gas saturation inside the core can be calculated from the CT images by the following equation

$$S_{gas} = \frac{CT_{preflush} - CT_{foam}}{CT_{preflush} - CT_{dry}} \quad (4)$$

where subscripts dry, preflush, and foam stand, respectively, for the dry core, core at the end of surfactant preflush before foam injection, and core with foam flow.

2.3. Experimental Procedure. Core-flooding experiments were performed as follows. First, the core was evacuated for roughly 2 h and then flushed with CO₂ with 5.0 bar back-pressure to remove all air from the porous medium. Next, several pore volumes of brine were injected into the dry core while varying back-pressure up from 0 to 25 bar to dissolve any CO₂ remaining in the core and to ensure 100% saturation core with brine. For the experiments in the absence of oil, a surfactant preflush was done prior to foam flooding. For experiments involving an EOR process, oil injection followed by water flooding and, subsequently, preflush of surfactant solution of the foaming agent were undertaken before foam flooding. Table 3 summarizes the procedures used for the experiments in the absence and presence of oil.

Table 3. Sequence and Conditions of Injection Step Used for the Core-Flooding Experiment

injection step sequence	flow rate (cm ³ /min)	back-pressure (bar)	injection direction
to evaluate the foam strength			
CO ₂ flushing to remove air	>20	5	downward
core saturation with brine	1.0–6.0	25	upward
surfactant preflush	1	30	upward
foam flooding (coinjection)	0.55	30	downward
for EOR process			
CO ₂ flushing to remove air	>20	5	downward
core saturation with brine	1.0–6.0	25	upward
oil injection (drainage)	0.5	5	downward
bump flood (oil)	8.0		
water flooding (imbibition)	0.5	5	upward
bump flood (brine)	5.0		
surfactant preflush	1	30	upward
foam flooding (coinjection)	0.6	30	downward

The first objective of the series of experiments was to examine the capability of the three selected surfactant solution formulations to

generate a stable foam. The chemical formulations, used for the foam flooding experiment in the absence of the oleic phase and for EOR experiments, are presented in Table 4. For each alkali–surfactant (AS) solution, core-flood experiments consisted of a coinjection of AS solution and N₂ in the absence of oil at room temperature. A surfactant solution was first preflushed to quench the surfactant adsorption of the core plug to reduce the effect of surfactant adsorption during foam flooding.

Foam flooding experiments were carried out by coinjecting nitrogen and surfactant solution while keeping the back-pressure at 30 bar. N₂ was injected from a cylinder at 50 bar to the mass-flow controller. The experiment was conducted under a back-pressure of 30 bar to minimize gas compressibility effects. Foam was generated by coinjecting N₂ and surfactant solution from the top of the sandstone core at a fixed total flow rate of 0.6 cm³/min. This flow rate is equivalent to a superficial velocity of 0.78 m/day [2.54 ft/day]. Foam floods were all carried out at a foam quality (i.e., inlet gas fractional flow) of 80%. The resistance to gas flow during foam generation and coalescence in the transient and steady-state conditions was evaluated macroscopically using the foam mobility reduction factor (MRF). Pressures of the generated foam and reference condition were measured to define $MRF = \Delta P_{foam} / \Delta P_{ref}$ as the ratio of pressure drops for foam flooding to single-phase water injection at the same flow rate.

3. RESULTS AND DISCUSSION

3.1. Foam Flow in Porous Media in the Absence of Oil.

3.1.1. Mobility Reduction Factor (MRF). Figures 2, 3, and 4

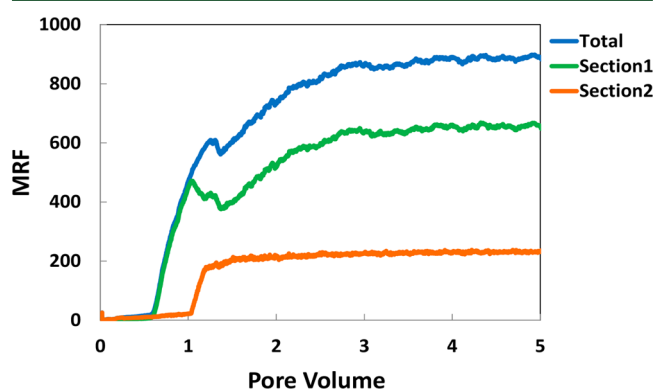


Figure 2. Total and sectional MRF results along the core from the experiment of coinjection of N₂ and AS1 surfactant in the absence of oil phase. Foam quality of 80%, and total velocity of 2.54 ft/day (section 1:11 cm from the injection point of the core; section 2:4.3 cm from the middle of the core to the outlet direction).

show the overall and sectional MRF vs numbers of PV obtained from the coinjection of N₂ and three formulates AS solutions along the core as a function of a number of coinjected pore volumes. MRFs for three cases after approximately 2 PV injections reach the plateau after 894, 567, and 282 with only a slight increase in the continuation of the test.

Table 4. Surfactant Formulations Used in Foam Strength Test and Oil Displacement Experiments

exp.	type of exp.	surfactant formulation	electrolyte composition	viscosity (cP)	density (g/cm ³)	IFT with hexadecane (mN/m)
AS1	foam flood	0.5 wt % AOS	2 wt % NaCl, 1 wt % Na ₂ CO ₃	1.12	1.05	1.56 × 10 ⁰
AS2	chemical-foam flood	0.2 wt % AOS + 0.6 wt % IOS	2 wt % NaCl, 1 wt % Na ₂ CO ₃	1.22	1.08	3.42 × 10 ⁻¹
AS3	chemical-foam flood	0.2 wt % AOS + 0.6 wt % IOS + 0.4 wt % cosolvent	2 wt % NaCl, 1 wt % Na ₂ CO ₃	1.18	1.10	1.17 × 10 ⁻²

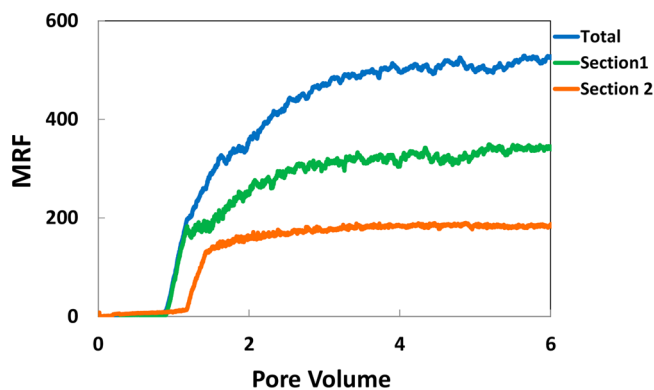


Figure 3. Total and sectional MRF results along the core from the experiment of coinjection of N_2 and AS2 surfactant in the absence of oil phase. Foam quality of 80%, and total velocity of 2.54 ft/day (section 1:11 cm from the injection point of the core; section 2:4.3 cm from the middle of the core to the outlet direction).

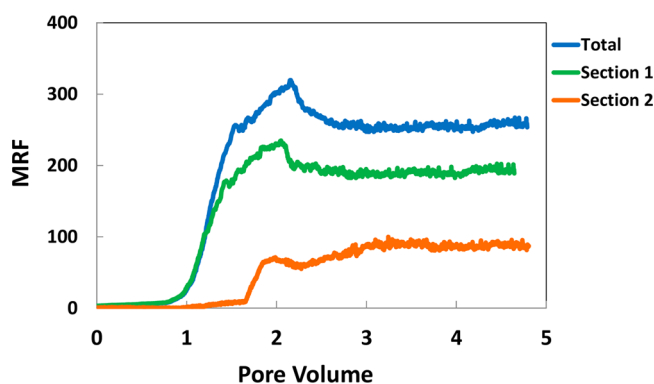


Figure 4. Total and sectional MRF results along the core from the experiment of coinjection of N_2 and AS3 surfactant in the absence of oil phase. Foam quality of 80%, and total velocity of 2.54 ft/day (section 1:11 cm from the injection point of the core; section 2:4.3 cm from the middle of the core to the outlet direction).

In all experiments it was found that about one pore volume in total was needed before strong foam was generated. At early injection times, coarse foam generation occurred, which provides only small pressure drops. The delay in foam generation and an increase of MRF can be attributed to competition between foam creation and destruction along the pores before reaching the minimum pressure gradient to create strong foam (Rossen and Gauglitz, 1990; Tanzil et al., 2002). Comparison of steady-state MRFs in Figures 2, 3, and 4 indicates AS1 has a higher MRF than AS2 and AS3, which demonstrates a much lower effect of IOS surfactant on the foam strength than AOS. Results also show that the lowest IFT formulation (AS3) enables foam generation with moderately high strength. The higher MRF of section 1 than section 2 is due to a longer distance of foam development and propagation along the core. By having evidence of the lowest IFT formulation to create a fairly stable foam in the absence of oil, this formulation (AS3) was chosen for the CT scan analysis.

3.1.2. CT Scans and Saturation Profiles. For the CT scan study, the experiment with the AS3 chemical formulation with the smallest MRF and a moderate strength of foam was chosen to investigate the stability of foam front propagation and the evolution of gas saturation. Figure 5 shows CT images taken during foam flooding in Bentheimer sandstone previously saturated with surfactant solution. The light blue color indicates

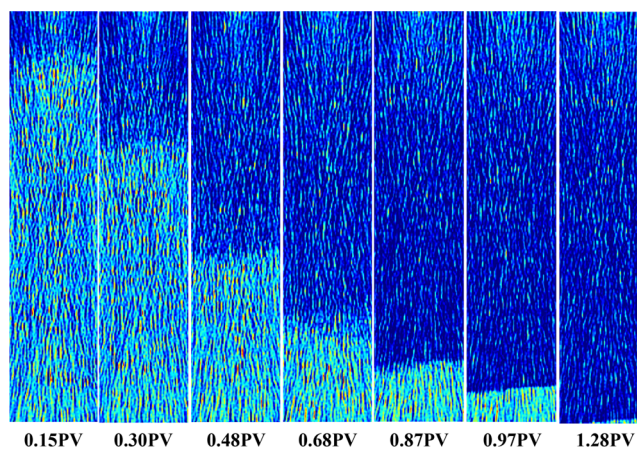


Figure 5. CT images obtained during coinjection of N_2 and chemical-foam agent (AS3). Foam flow was studied in a single core of Bentheimer sandstone. First sharp foam front advances through the core after about 0.8 PV injection. Sharp front of generated foam is evident of stable foam displacement in the core.

a core fully saturated with a surfactant solution, and the change to dark blue corresponds to the foam phase. Images clearly show the advancement of foam from the top to the bottom of the core.

The number below each image represents the number of foam pore volumes injected (elapsed time). Images show that foam displaces surfactant solution in a piston-like manner, indicating that a more viscous fluid (i.e., foam) is displacing a less viscous fluid in a stable manner. Color changes from light blue to dark blue from the left to right give evidence of the increase of gas saturation behind the front. There is a small region near the inlet face with a relatively higher intensity of light blue color, which remained for a while, indicating higher water saturation compared to the rest of the core. Discontinuity of capillary pressure at the inlet face results in the retention of the water phase, which is the wetting phase with respect to sandstone rock, at the core inlet. For further analysis, we plotted gas saturation profiles, obtained by eq 4, by combining the CT scans for dry core, core fully saturated with surfactant solution, and core during foam injection. Gas saturation was obtained by the arithmetic average of every horizontal line of the saturation voxel throughout one CT image slice. Gas saturation for foam flooding with very low IFT surfactant formulation (AS3) is plotted in Figure 6 against different coinjection pore volumes.

The inlet effect, with a high water saturation near the core inlet over a length of approximately 2.5 cm, was observed in Figure 6 and persisted over the entire duration of the experiment. It can be explained by the discontinuity of capillary pressure at the injection face of the core, due to the fact that the foam phase, including a high fraction of the nonwetting phase (gas), displaces the wetting phase (surfactant solution). This creates a large capillary pressure contrast before the inlet, which is outside of porous media, where the capillarity is zero. Foam saturation profiles consist of a downward-concave shape and a horizontal part. At early times, for instance, 0.1 PV, gas saturation is below of 0.40 and then rises and reaches the average value of approximately 0.65. A progression of gas saturation curves illustrates a typical Buckley–Leverett front shape, including the effect of gas compressibility and capillarity. By the progression of the foam flow and subsequently increasing gas mobility reduction factor (MRF), the capillary

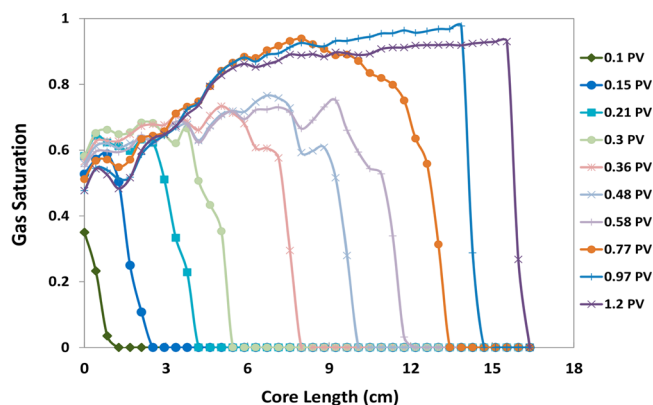


Figure 6. Gas saturation profiles taken at every vertical position throughout the core before and after foam breakthrough (BT) obtained from the CT images shown in Figure 5. Foam quality at the inlet face of the core was 80%. Rapid in situ foam generation and fairly piston-like front for the gas saturation propagation were observed.

pressure can be overcome by the foam propagation. This results in the wetting phase (i.e., water) being displaced by the foam, which has 80% gas saturation. Thus, the gas saturation becomes higher when the core length exceeds 6 cm.

3.2. Displacement of Oil by Foam. **3.2.1. Drainage and Imbibition.** Primary drainage and imbibition are reported here, prior to discussing oil recovery by foam. Oil was injected into the core, previously fully saturated with brine at a velocity of 2.24 ft/day, until no water was flowing out of the system. Then oil saturation was measured, either by analyzing CT scan images or by measuring the volume of the effluents. For the first and second experiments (AS1 and AS2), the saturation was determined from the mass balance calculation of the measured effluent volumes of oil and water. CT scans of the cores were executed throughout the whole experiment at time intervals for the third experiment (AS3) to determine precisely the in situ saturations of water and oil in addition to mass balance calculation of the effluent. The overall and sectional pressure drops along the core during drainage are plotted in Figure 7. When oil was introduced to the inlet of the core, pressure drops abruptly raised. The sharp increase is characteristic of the entry capillary pressure between water and oil according to the Young–Laplace equation ($P_{c_in} = 2\sigma_{ow} \cos(\theta)/r$).

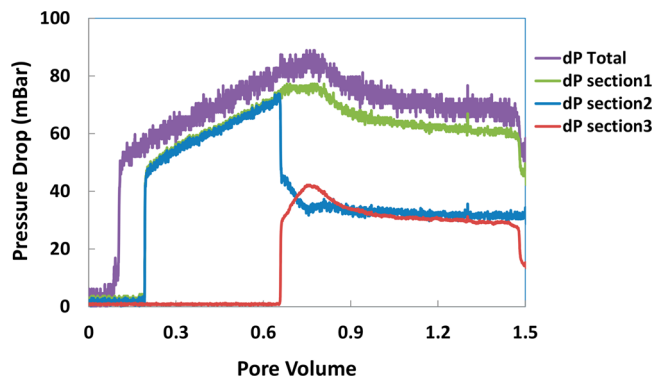


Figure 7. Pressure drop profiles during primary drainage over the core and different section of the core (section 1:11 cm, section 2:4.3 cm, and section 3:4.75 cm). Oil was injected at $0.5 \text{ cm}^3/\text{min}$ under gravity-stable conditions. Initial jump in the pressure drop profiles corresponds to the entry capillary pressure.

Figure 8 shows a series of CT scan images taken at different times during primary drainage. The blue color corresponds to a

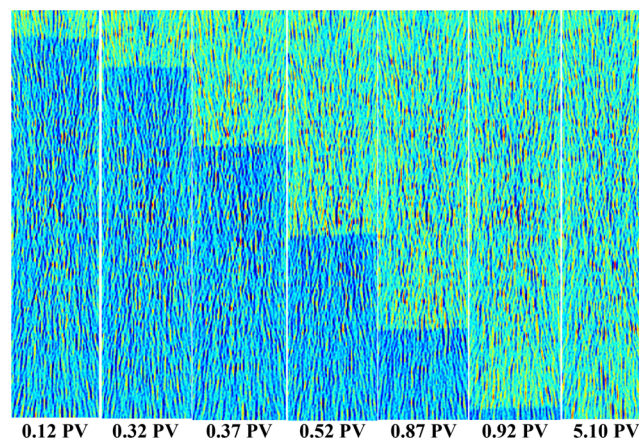


Figure 8. Displacement profile during primary drainage (oil injection) with injection direction from top to bottom. Water phase (blue color) was displaced by oil (light green).

core fully saturated with brine, while the light green color corresponds to the presence of the oleic phase. Oil is injected from the top to the bottom of the core, so that the color of the image varies from blue to light green from the left to right. The displacement is gravity stable with a rather sharp front between the oil and the water phase. The CT images were further analyzed to quantify the oil saturation map at different PV injected. Oil saturation was calculated from the CT images according to eq 4 by combining the images for the dry core, the fully brine-saturated core, the bulk attenuation coefficient of oil, and the brine.

Changes in oil saturation, plotted in Figure 9, are in a piston-like profile and consistent with Buckley–Leverett theory for

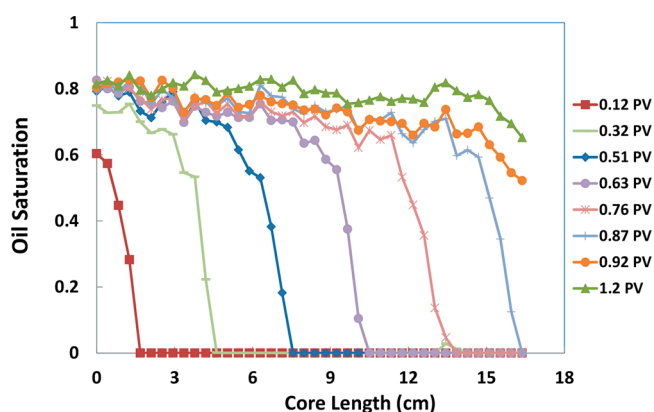


Figure 9. Oil saturation profile for oil injection as a primary drainage obtained from the corresponding CT images shown in Figure 8. Oil was injected from the top of the core, which is located on the left side of the figure. Average oil saturation at the end of primary drainage was 0.80 ± 0.02 .

two-phase flow.^{24–28} When no more water was observed at the outlet, bump flood oil injection at a flow rate of $8 \text{ cm}^3/\text{min}$ was performed to reach connate water saturation. At the end of the primary drainage, the average oil saturation in the core was $S_o = 0.81 \pm 0.02$, and thus, connate water saturation was $S_{wc} = 0.19 \pm 0.02$ (see Figure 9). After drainage, the core was subjected to water flooding (imbibition) at a flow rate of $0.5 \text{ cm}^3/\text{min}$, equal

to the interstitial velocity of 2.24 ft/day, until no more oil was produced from the core. The sectional pressure drops and the total pressure drop over the core during water flooding are shown in Figure 10.

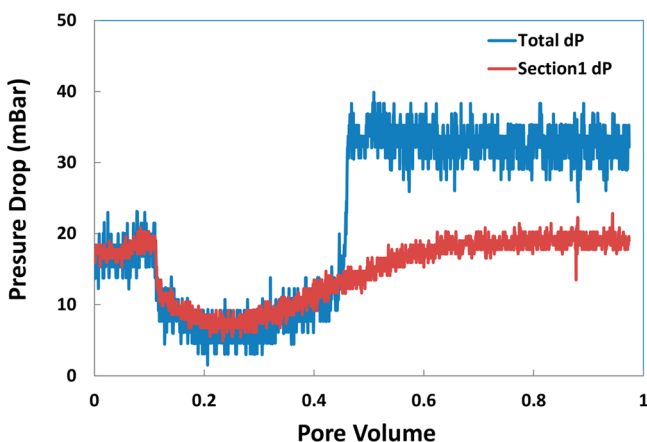


Figure 10. Total and sectional pressure drop profile during water flooding at $0.5 \text{ cm}^3/\text{min}$ during the first two pore volumes injected. Water BT coincides with the time at which pressure drop obtains a maximum value.

As imbibition was introduced into the core inlet, the pressure drop decreased, indicating the capillary pressure between the two phases declined, due to the presence of wetting phase (water) at the front. Pressure drop behavior is characteristic of imbibition in a water flooding process with an early water breakthrough (BT) at 0.38 PV, accompanied by a long tailing oil production as the total pressure drop gradually levels off to a plateau. This is consistent with CT images of this test shown in Figure 11, where a BT time close to 0.33 PV was determined.

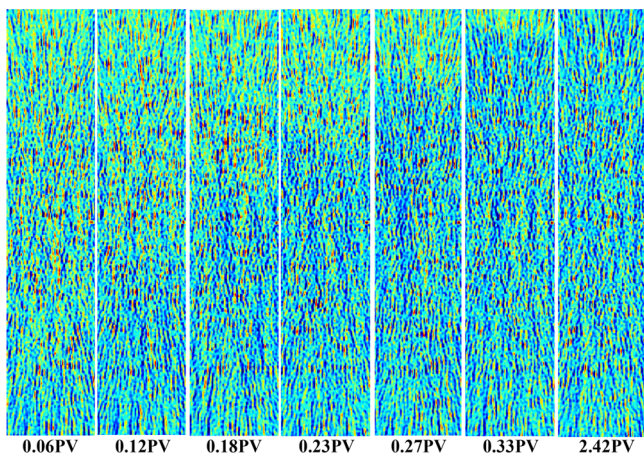


Figure 11. Displacement profile during gravity-stable water flooding (imbibition) with injection direction from the bottom to the top. Oil production by water flooding is evident by a color change from light green to blue.

Figure 11 demonstrates, during the imbibition, that change color of the images from left to right changes from light-green to a blueish tint, which reflects the removal of oil. Fingering and bypassing of oil by brine are also visible in the images. Figure 12 shows the oil saturations obtained by applying eq 3 and using the CT scan images that were presented in Figure 11. The oil saturation front is wide, due to capillary diffusion and an

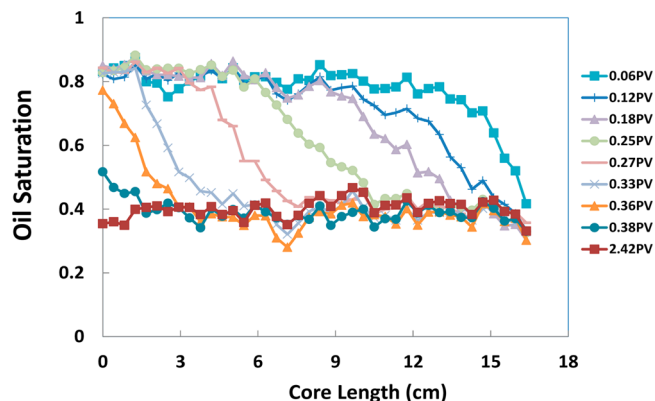


Figure 12. Profile of oil saturation distribution for water flooding obtained from the corresponding CT images given in Figure 11. Brine was injected from the bottom of the core, which is located on the left side of the figure. Average oil saturation at the end of water flooding was 0.4 ± 0.02 .

unfavorable mobility ratio between displacing and displaced phases. The water flooding was followed by bump flood, i.e., by brine injection at $5.0 \text{ cm}^3/\text{min}$ to ensure that a residual oil saturation was reached. The last CT image was taken after bump water flooding, which gave $1.7 \pm 0.1\%$ of the OIIP. By doing this the remaining oil saturation reached an average of $S_{or} = 0.4 \pm 0.02$.

3.2.2. Oil Recovery by Chemical-Foam Flooding.
3.2.2.1. Foam Strength. Prior to chemical-foam flooding the core was preflushed by 3.0 PV of alkali-surfactant (AS) solution at the same flow rate as water flooding. This was done to satisfy the adsorption capacity of the core surface, thus preventing loss of surfactant and the delay in foam generation due to adsorption. During surfactant preflush, only a tiny amount of oil of about $0.5 \pm 0.1\%$ of the OIIP was produced. Subsequently, N_2 and surfactant solutions were injected into the core. The MRFs obtained during foam flooding for the three cases of the chemical formulations (see Table 4) are depicted in Figures 13, 14, and 15. Here MRF is defined as the ratio of pressure drops for foam flooding to a single-phase water injection at the same flow rate. AS1 demonstrated a sharp increase in MRF after 0.7 PV, while AS2 and AS3 tests provided smaller steady-state MRF in the oil recovery experiment, since the solutions used in these two experiments contained a lower

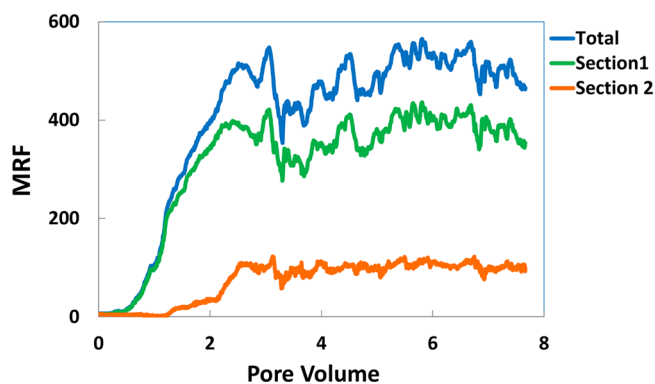


Figure 13. Total and sectional MRF results along the core from the experiment of coinjection of N_2 and AS1 surfactant solution in the presence of remaining oil after water flooding. Foam quality of 80%, and total velocity of 2.5 ft/day.

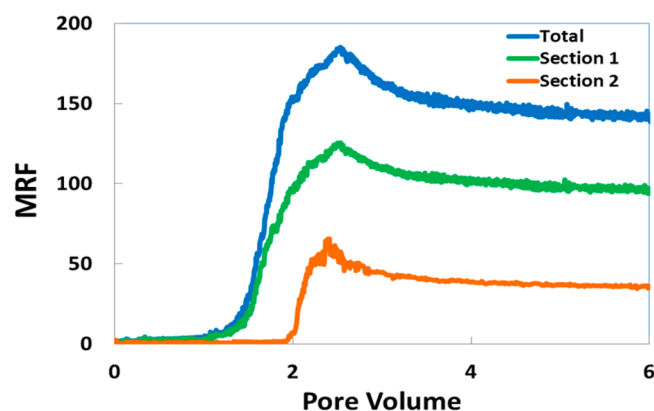


Figure 14. Total and sectional MRF results along the core from the experiment of coinjection of N_2 and AS2 surfactant in the presence of remaining oil after water flooding. Foam quality of 80%, and total velocity of 2.5 ft/day.

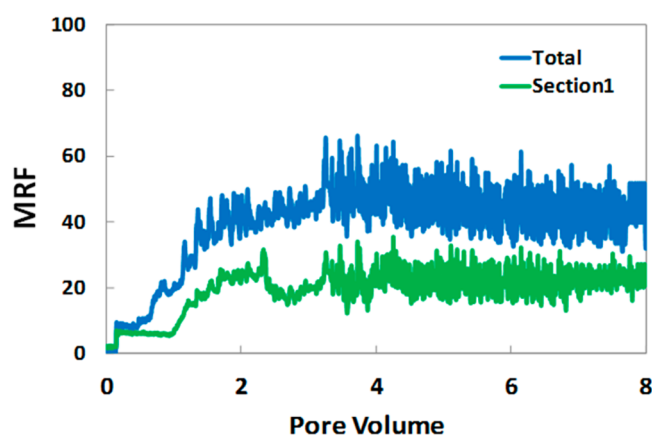


Figure 15. Total and sectional MRF results along the core from the experiment of coinjection of N_2 and AS3 surfactant solution in the presence of remaining oil after water flooding. Foam quality of 80%, and total velocity of 2.5 ft/day.

amount of AOS surfactant. For AS2 beyond 1.2 PV, MRF increased progressively and then leveled off to approximately 165. The average MRF during coinjection of N_2 with AS3 was rather low, which means that moderately stable foam was generated in the core under a considerably low IFT condition and in the presence of high residual oil saturation. The MRF fluctuation in Figure 15 was due to the wide range of pressure difference measurement (from -40 to $+40$ bar).

3.2.2.2. CT Scanning Images. For the experiment AS3 the core was CT scanned during foam flooding at transient and steady-state conditions in order to discern the effects of the ultralow IFT between the oil and the aqueous phase. The corresponding CT scan images are shown in Figure 16. The light blue-green color corresponds to the core containing surfactant solution and residual oil. Dark blue indicates the presence of foam. As gas (N_2) and the surfactant were coinjected downward into the core, foam propagation is clearly visible in a change of the intensity of color from blue into a darker blue. This gives insight about a change of fluid saturation from the two-phase regions into the three-phase regions (i.e., oleic phase, surfactant solution, and foamed gas). CT images, shown in Figure 16, clearly confirm the ability of foam flooding of AS3 to displace a substantial volume of the liquid-phase consisting oil.

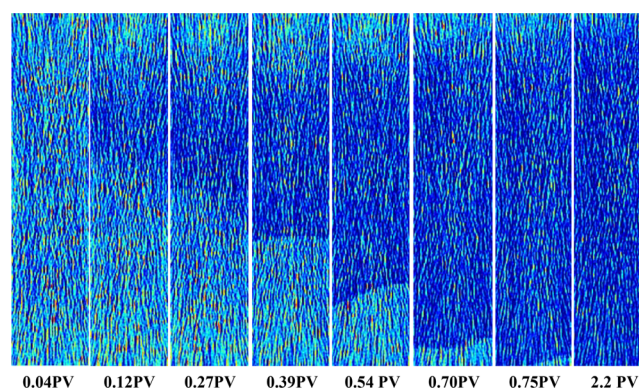


Figure 16. CT images obtained during AS3 chemical-foam flooding. Foam BT occurred at $0.76 \text{ PV} \pm 0.03 \text{ PV}$. Dark blue color indicates the presence of foam phase.

Near the core inlet, over approximately 2.4 cm, a light blue/green color remained for a long time after coinjection started indicating the persistence of high liquid saturations in the core inlet region. This was observed by others (Nguyen et al., 2007; Simjoo and Nguyen, 2011) and can be explained by the fact that the foam strength is too small to displace liquid. After the inlet face of the core, until 0.39 PV, we see that in the area, for approximately 10.5 cm distance, the foam texture is coarse and the foam is not yet fully developed, because the injected gas needed to travel a certain distance to reach a minimum pressure gradient before strong foam generates. As a result, a low amount of the liquid phase is displaced and no sharp front of gas flow together with the liquid as the foam phase formed.

According to both the CT images shown above and the perspective of the population balance approach (Falls et al., 1988; Kovscek et al., 1997), we could argue that total densities of flowing and stationary bubbles from the core inlet increase toward a certain value based on dominating parameters like oil saturation. It is also illustrated that as oil saturation varied during incremental oil recovery, subsequently the transient foam propagation was influenced. In addition, according to the oil cut plot shown later in Figure 18, there should be an oil bank formed behind the gas BT. As shown in Figure 16, in the region of an advancing front from a 0.39 PV, a sharp front is characterized by a clear change in the image color from light blue-green color to dark blue. This region progressed over the core length by creating a sharp front in continuation, which indicates formation of a fairly strong foam. The CT images demonstrate excellent foam development: foam propagated as a sharp front until it reached the outlet face; moreover, the generated foam was strong enough to induce a gradual reduction of the liquid phase and oil saturations. This can be clearly seen from the color change in the lower part (oil-bearing) of the core from, the light blue to a more intense blue. Recall the dark blue color, indicating the presence of stronger foam and, consequently, a larger liquid desaturation. Thus, the CT core-flood experiment of AS3 proved that stable foam can be generated using a chemical formulation, which provides ultralow IFT between the oleic and liquid phases. Figure 17 shows the total gas saturation corresponding to foam flow through the water-flooded section in which a three-phase (gas, oil, surfactant solution) flow occurred.

In this plot, the resulting average gas saturation profiles, as a function of the height of the rock sample, are illustrated. Gas saturation values are arithmetic averages of gas saturation in

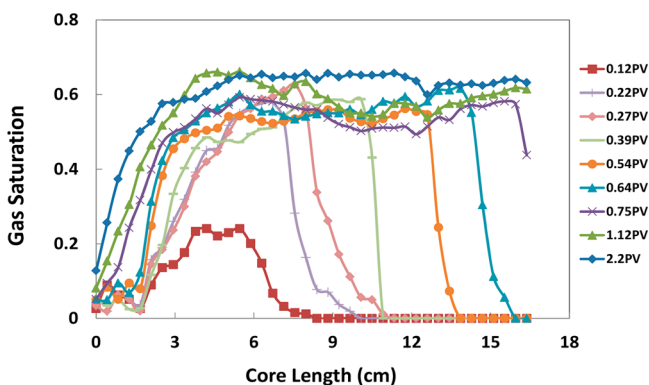


Figure 17. Gas saturation profiles taken at every vertical position throughout the core before and after foam BT obtained from the CT images shown in Figure 16.

each horizontal line over each cross section along the rock sample. Focusing on the saturation profile taken at 0.39 PV, the region discussed above on CT images, can be characterized as follows. Gas saturation in the first 2.4 cm is low, because of the inlet effect, where capillary discontinuity resulted in retention water phase. After this inlet region, where the liquid saturation remained high, gas saturation raised to an average value of 0.63 ± 0.05 and then diminished to zero, ahead of the foam front, between 5.2 and 17.0 cm, obviously $S_g = 0$. Figure 17, after foam BT, demonstrates a relatively constant saturation of $S_g = 0.65$ throughout the core with some minor fluctuations from this number. This shows that the amount of liquid is higher than in the case without oil (see Figure 6), which supports the idea that the presence of oil results in weaker foam. Furthermore, it can also be seen from Figure 17 that throughout the whole time of experiments gas saturation curves displayed a typical Buckley–Leverett shape, including the effect of gas compressibility.

3.2.2.3. Oil Recovery. We now analyze the tertiary oil recovery mechanism of three types of coinjection of surfactant solutions and gas that exhibited different properties in terms of foam mobility control and IFT reduction. To discern the oil recovery mechanism for each EOR experiment, we examined the performance of the process in terms of cumulative oil recovery and oil cut. The cumulative oil recovery factor was defined as the ratio of the produced oil to oil initially in place (OIIP) and the oil cut defined as the fraction of oil in the produced fluid. Oil cut and cumulative oil recovery for the three studied cases are presented in Figure 18 and Figure 19, respectively. During all foam flooding tests, in the first 1.0 PV, the oil cut (oil production rate) increased, whereas during the later time of the testing it decreased progressively. Oil was produced first by the formation of a diffuse oil bank followed by a long tail production. For AS1, as foam injection continued for a longer time than 1 PV of injection, oil recovery was at a slower rate and mainly as a stable emulsion. An early oil BT was observed during the AS1 experiment, at approximately 0.3 PV (see Figure 18), which is attributed to a poor oil displacement before the oil bank is formed. For the AS2 and AS3 experiments, oil BT time was consistently longer, corresponding to the formation of oil with a sharper bank and a more stable oil displacement. Figure 19 indicates that for AS3 oil production was larger with a higher rate and more slowly in terms of BT of the oil bank than others, although the MRF created by foam generation was the lowest (see Figure 15).

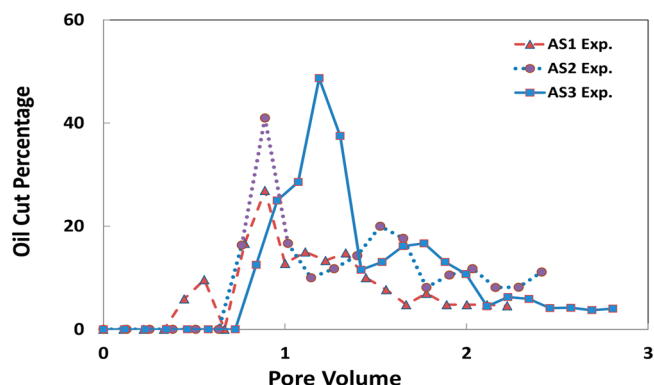


Figure 18. Oil cut during foam flooding with different AS formulations (AS1, AS2, and AS3). Effect of IFT reduction on fraction flow of oil recovery can be seen. First oil peaks are corresponding to oil bank formation.

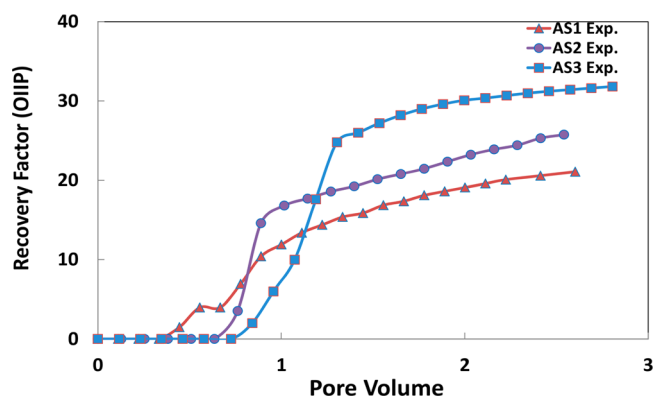


Figure 19. Incremental oil recovery during foam flooding for different surfactant concentrations. Increased cumulative oil recovery was observed for lower IFT foam flooding.

Table 5 gives a summary of incremental oil recovery by coinjection of N_2 with three different chemical formulations investigated. For AS1, the cumulative oil effluent measurement indicated an oil recovery factor up to 22% of OIIP after injection of 2.5 PV of foam. For the AS3 case, injection of 2.5 PV of foam yielded an incremental oil recovery of 34% of OIIP. Since oil recovery by water flooding was $43 \pm 0.05\%$, the overall oil recovery of foam flooding is $77.00 \pm 0.05\%$ OIIP. The results show that a decrease in the IFT led to substantially higher oil recovery consisting with lower MRF (see Figures 13 and 15).

The oil recovery increases substantially for AS3, when the IFT decreases compared to conventional foam flooding (AS1) EOR. Thus, in the case of AS3 foam, ultralow IFT reduction was the dominant mechanism in comparison to AS1 for the higher oil recovery. In Figure 20 a comparison of part of the oil recovery in effluents by foam flooding for experiments AS1 and AS3 is shown. As can be seen produced oil by AS3 gave a more clean oil than AS1 and that with AS1 a noticeable amount of oil production was including the emulsion formation.

4. CONCLUSIONS

- The oil displacement efficiency by chemically designed foam flooding was investigated experimentally. Three chemical formulations (AS1, AS2, AS3) capable of generating stable foam in porous media in the absence

Table 5. Summary of Incremental Oil Recovery by Coinjection of Gas with Different Chemical Solutions

EOR process	S_{oi}	$R_{F,WF}$ (OIO)	$S_{or,WF}$	$R_{F,EOR}$ (OIO)	$S_{or,EOR}$	MRF	IFT (mN/m)	foam BT time (PV)
AS1	0.80 ± 0.05	40 ± 1	0.48 ± 0.02	21.1 ± 1	0.32 ± 0.02	570 ± 5	1.56×10^0	0.81 ± 0.02
AS2	0.83 ± 0.05	44 ± 1	0.47 ± 0.02	27.5 ± 1	0.25 ± 0.02	165 ± 5	2.42×10^{-1}	0.79 ± 0.02
AS3	0.81 ± 0.05	43 ± 1	0.46 ± 0.02	33.7 ± 1	0.20 ± 0.02	59 ± 5	1.17×10^{-2}	0.76 ± 0.02

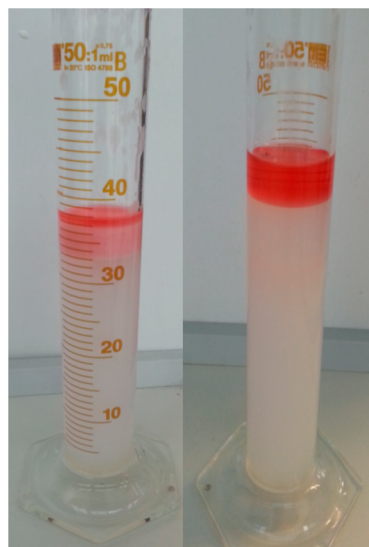


Figure 20. Fluids at the outlet of the core for the AS1 foam (left image) and AS3 foam (right image). Oil is colored red to visualize. Produced oil at the effluent of AS1 foam appearing more as an emulsion with surfactant solution. Clean oil is much more for AS3 foam. Larger liquid volume in the right column is because of longer surfactant preflush.

and presence of oil, while reducing the IFT to the low and ultralow values, have been examined.

- Core floods were performed using AS formulations providing low to ultralow oil/water IFT in addition to being good foaming agents with nitrogen into Bentheimer sandstone.
- The foaming of the three AS formulations in consolidated porous media in the absence of oil gave rise to gas mobility factors ranging from 894 to 282.
- A blend of two anionic surfactants with a cosolvent (AS3) was developed, both to increase MRF and to decrease the IFT by at least 3 orders of magnitude. Experiments with the AS3 chemical formulation in the absence and presence of oil were monitored by an X-ray CT scanner and during foam propagation demonstrated a stable foam front and liquid desaturation movements. CT images elucidated the transient foam flow behavior, which is the most relevant to enhanced oil recovery.
- The chemical-foam flooding exhibited the similar characteristic of ASP flooding EOR such as the production of large oil bank at high oil cut before producing oil/emulsion. The obtained results proved that microscopic displacement efficiency in foam flooding can greatly be improved by reducing capillary pressure.
- The obtained results were compared against the typical AOS foam flooding as a base case (AS1) and resulted in the higher oil recovery and significantly less MRF for the low-IFT foam than the base-case experiment. A considerable portion of oil recovered in AS1 experiment

formed oil-in-water emulsion, but produced oil by AS3 gave a much more clean oil cut. These results indicated the importance of lowering IFT during foam EOR and the necessity of having only a sufficient foam strength. This means that ultrastrong foam is not necessary to prevent a detrimental destabilization effect of oil on foam.

- This research demonstrated that the low microscopic efficiency of foam flooding is due to bypassing of trapped oil due to high capillary pressure. Fairly low IFT foam flooding (AS2, AS3) recovered oil at the tertiary stage by a mechanism of improving volumetric sweep efficiency and increasing microscopic oil displacement.
- For future work, conducting the foam flow experiments at reservoir conditions, such as reservoir temperature and pressure, and formation wettability (oil-wet, mixed-wet) will more accurately reflect the foam behavior during chemical-foam flooding for oil displacement. Moreover, in addition to using blend of surfactants and cosolvent the addition of viscosifying agent like polymer to AS slug and foam drive is worth investigating for the chemical-foam EOR process.

AUTHOR INFORMATION

Corresponding Author

*E-mail: S.M.HosseiniNasab@tudelft.nl, Hosseininasab100@gmail.com.

ORCID

S. M. Hosseini-Nasab: 0000-0001-5429-1796

Notes

The authors declare no competing financial interest.

ACKNOWLEDGMENTS

We acknowledge the financial support from the Ministry of Science, Research and Technology of Iran for the research study in this work. We are very thankful to Shell Global Solution BV for providing us chemicals, and greatly thanks to Dr. Hassan Mahani and Mr. Hilbert van der Linde for their supports to perform experiments in the Rock & Fluid Physics Laboratory of Shell Global Solution BV at Rijswijk, Netherlands. We thank M. Friebel, E. Meivogel, and M. Slob for technical support at the Dietz Laboratory of the Geoscience and Engineering Department, TU Delft. We appreciate Dr. C. Boeije, the University of Bordeaux, for a careful reading of the manuscript and providing us valuable comments.

REFERENCES

- (1) Lake, L. W.; Russell, J.; Rossen, B. *Fundamentals of Enhanced Oil Recovery*; Society of Petroleum Engineers, 2014; http://txessarchive.org/documents/J_EOR_ppt.pdf (Accessed Feb 1, 2015).
- (2) Mannhardt, K.; Schramm, L. L.; Novosad, J. J. Effect of Rock Type and Brine Composition on Adsorption of Two Foam-Forming Surfactants. *SPE Adv. Technol. Ser.* **1993**, *1*, 212–218.
- (3) Rossen, W. R. Marcel Dekker: New York, 1996.

- (4) Schramm, L. L.; Smith, D. H. *Foams: Fundamentals and Applications in the Petroleum Industry*; American Chemical Society: Washington, DC, 1994.
- (5) Huh, D. G.; Handy, L. L. Comparison of Steady- and Unsteady-State Flow of Gas and Foaming Solution in Porous Media. *SPE Reservoir Eng.* **1989**, *4*, 77–84.
- (6) Hosseini-Nasab, S. M.; Zitha, P. L. J. Investigation of certain physical–chemical features of oil recovery by an optimized alkali–surfactant–foam (ASF) system. *Colloid Polym. Sci.* **2017**, DOI: 10.1007/s00396-017-4162-1.
- (7) Guo, H.; Zitha, P.; Faber, R.; Buijse, M. A Novel Alkaline/Surfactant/Foam Enhanced Oil Recovery Process. *SPE J.* **2012**, *17*, 1186–1195.
- (8) Li, R. F.; Hirasaki, G. J.; Miller, C.; Masalmeh, S. K. Wettability Alteration and Foam Mobility Control in a Layered, 2D Heterogeneous Sandpack. *SPE J.* **2012**, *17*, 1207–1220.
- (9) Yuqiang, P.; Dehuang, S.; Shaocheng, X. Experimental study on nitrogen foam flooding to enhance oil recovery in heavy oil reservoir-taking Qinhuangdao 32–6 Oilfield with heavy oil as an example. *Pet. Geol. Recover. Effic.* **2008**, 59–61.
- (10) Kang, W.; Liu, S.; Meng, L.; Cao, D.; Fan, H. A Novel Ultra-low Interfacial Tension Foam Flooding Agent to Enhance Heavy Oil Recovery. In *Proceedings of SPE Improved Oil Recovery Symposium*; Society of Petroleum Engineers, 2010.
- (11) Hosseini-Nasab, S. M.; Padalkar, C.; Battistutta, E.; Zitha, P. L. J. Mechanistic Modeling of the Alkaline/Surfactant/Polymer Flooding Process under Sub-optimum Salinity Conditions for Enhanced Oil Recovery. *Ind. Eng. Chem. Res.* **2016**, *55*, 6875–6888.
- (12) Chevallier, E. et al. Foams with Ultra-Low Interfacial Tensions for an Efficient EOR Process in. (2015).
- (13) Tang, S.; et al. A Novel Low Tension Foam Flooding for Improving Post-Chemical-Flood in Shuanghe Oilfield. In *SPE Improved Oil Recovery Symposium*; Society of Petroleum Engineers, 2014.
- (14) Szlendak, S. M.; Nguyen, N.; Nguyen, Q. P. Laboratory Investigation of Low-Tension- Gas Flooding for Improved Oil Recovery in Tight Formations. *SPE J.* **2013**, *18*, 851–866.
- (15) Wu, W.; Pan, J.; Guo, M. Mechanisms of oil displacement by ASP-foam and its influencing factors. *Pet. Sci.* **2010**, *7*, 100–105.
- (16) Cui, L.; Ma, K.; Puerto, M.; Abdala, A. A.; Hirasaki, G. Mobility of Ethomeen C12 and Carbon Dioxide (CO₂) Foam at High Temperature/High Salinity and in Carbonate Cores. *SPE J.* **2016**, *21*, SPE-179726-PA.
- (17) Hosseini-Nasab, S. M.; Zitha, P. L. J.; Mirhaj, S. A.; Simjoo, M. A New Chemical-Enhanced Oil Recovery Method? *Colloids Surf., A* **2016**, *507*, 89–95.
- (18) Srivastava, M.; Nguyen, Q. Application of Gas for Mobility Control in Chemical EOR in Problematic Carbonate Reservoirs. *Proc. SPE Improv. Oil Recover. Symp.* **2010**, DOI: 10.2118/129840-MS.
- (19) Chabert, M. et al. A CO₂ Foam Conformance Pilot in US Gulf Coast Region. *Abu Dhabi International Petroleum Exhibition & Conference*, Nov 7–10, 2016, Abu Dhabi, UAE; Society of Petroleum Engineers, 2016.
- (20) Li, R. F. Foam Mobility Control for Surfactant Enhanced Oil Recovery. *SPE J.* **2010**, *15*, 20–23.
- (21) Ma, K.; Lontas, R.; Conn, C. a.; Hirasaki, G. J.; Biswal, S. L. Visualization of improved sweep with foam in heterogeneous porous media using microfluidics. *Soft Matter* **2012**, *8*, 10669.
- (22) Rossen, W. R.; Gauglitz, P. A. Percolation Theory of Foam in Porous Media. *AIChE J.* **1990**, *36*, 1176.
- (23) Tanzil, D.; Hirasaki, G. J.; Miller, C. A. Conditions for Foam Generation in Homogeneous Porous Media. In *SPE/DOE Improved Oil Recovery Symposium*; Society of Petroleum Engineers, 2002.
- (24) Willhite, G. P. *Waterflooding*; Society of Petroleum Engineers, 1986.
- (25) Simjoo, M.; Nguyen, Q. P. *Rheological Transition during Foam Flow in Porous Media*; Society of Petroleum Engineers, 2011.
- (26) Nguyen, Q. P.; Currie, P. K.; Buijse, M.; Zitha, P. L. J. Mapping of foam mobility in porous media. *J. Pet. Sci. Eng.* **2007**, *58*, 119–132.
- (27) Falls, A. H. Development of a Mechanistic Foam Simulator: The Population Balance and Generation by Snap-Off. *SPE Reserv. Eng.* **1988**, *3*, 884–892.
- (28) Kovscek, A. R.; Tadeusz, W. P.; Radke, C. J. Mechanistic Foam Flow Simulation in Heterogeneous and Multidimensional Porous Media. *SPE J.* **1997**, *2*, 511–526.